Received 15 November 2023; revised 13 December 2023; accepted 21 December 2023. Date of publication 25 December 2023; date of current version 26 March 2024.

Digital Object Identifier 10.1109/OJAP.2023.3347083

A Dual-Polarized and Wideband Switchable Absorption/Transmission Frequency Selective Surface With Multispectral Functionality

HUANGYAN LI [1] (Member, IEEE), YOUYI FENG [1], MINXIN ZHAO [2], XIANG WANG [1] (Member, IEEE), DANILO BRIZI [3] (Member, IEEE), XIAOXING FANG [4] (Member, IEEE), JUN HU [1] (Member, IEEE), BOYU SIMA [1] (Member, IEEE), ZHIYUAN ZONG [1] (Member, IEEE), WEN WU [1] (Senior Member, IEEE), AND AGOSTINO MONORCHIO [3] (Fellow, IEEE)

[1]School of Electronic and Optical Engineering, Nanjing University of Science and Technology, Nanjing 210094, China

[2]Department of Electronic and Information Engineering, Nanjing University, Nanjing 210093, China

[3]Department of Information Engineering, University of Pisa, 56122 Pisa, Italy

[4]School of Electronic and Information Engineering, Nanjing University of Information Science and Technology, Nanjing 210044, China

CORRESPONDING AUTHOR: H. LI (e-mail: huangyan_lee@163.com)

This work was supported in part by the National Natural Science Foundation of China under Grant 62301256, Grant 62201262, Grant 62101262, and Grant 62201269; and in part by the Key Laboratory of Radar Imaging and Microwave Photonics (Nanjing University of Aeronautics and Astronautics), Ministry of Education under Grant NJ20210002.

ABSTRACT In this paper, a microwave absorption/transmission switchable frequency selective surface (A/T-SFSS) with enhanced multispectral functionality in the visible and infrared spectra is developed. By simply controlling the flowing liquid medium (pure water in this work), efficient manipulation of two opposite states, absorption and transmission, can be achieved in the microwave frequency band with a wide switchable bandwidth. When functioning as a wideband absorber, the proposed A/T-SFSS exhibits an absorption rate over 90% from 6.50 GHz to 10.48 GHz. Conversely, it can be employed as a transmitter with high selectivity, featuring a second-order passband with two transmission zeros at both sides and an impressive −1 dB transmission bandwidth ranging from 7.04 GHz to 8.47 GHz. The design also demonstrates stable responses under different polarizations and incident angles. Additionally, the proposed A/T-SFSS offers flexibility in tailoring the visible and infrared spectra by actively changing the color and temperature of aqueous solutions. The influences of electromagnetic (EM) parameters and liquid temperature variations on the microwave performance are also thoroughly investigated. Finally, experimental verification through free-space tests of scattering parameters, image analyses of grayscale histogram, and infrared radiation detected by thermal imager provides compelling evidence for the potential of the developed A/T-SFSS. The results demonstrate its remarkable capability to achieve switchable microwave functionality as well as active control of visible light and infrared spectra, which significantly contributes to the field by advancing the development of multifunctional and multispectral structures.

INDEX TERMS Frequency selective surface (FSS), multispectral, switchable microwave function, visible light camouflage, infrared radiation management.

I. INTRODUCTION

DUE TO their effectiveness in attenuating electromagnetic (EM) waves, EM absorbers have become indispensable components in modern EM engineering and hold immense potential for future advancements in various disciplines [1], [2], [3], [4].

In recent years, some absorbers based on water medium have been reported [5], [6], [7], [8], [9], [10], [11], [12], [13], [14], [15]. Compared to traditional metamaterial absorbers, these water-based absorbers can achieve wider bandwidth and higher efficiency in terms of absorbing performance owing to the dispersive and lossy characteristics of water. Further, water-based designs with reconfigurable functions, which are more adaptable to the rapidly changing and increasingly complex EM environment, can be achieved based on the liquid fluidity [16], [17], [18], [19], [20]. In [16], a water-based tunable metamaterial is first designed and its tunability is realized by rotating the functional device, which reshapes the water inside the reservoir. Wideband tunable absorbers based on the combination of indium tin oxide (ITO) resonant patterns and water substrates are proposed in [17], [18], and the absorption rates can be tuned by altering the thicknesses of homogeneous water layer. A water-based structure comprising spherical fluidic channels is presented in [19], and the switchable function between absorption and reflection can be attained by controlling the status of liquid injection. After that, a wideband absorber/reflector based on the stacking technique and super-element configuration is developed, which enhances the modulation bandwidth of both absorption and reflection states [20].

To date, most switchable absorbers previously reported are of the absorption/reflection type. The concept of frequency selective radar absorber (FSR), which combines in-band transmission and out-of-band absorption functionalities, has been extensively researched in recent decades [21], [22], [23]. Several FSR designs have been developed with reconfigurable capabilities that allow for dynamic switching within the passband [24], [25]. However, there are very few reconfigurable designs that can integrate the exact opposite states of absorption and transmission within the same operating band since a reflective ground plane is usually required in designing absorbers. Based on the active frequency selective surface (FSS) configuration, an absorption/transmission switchable surface is designed to simultaneously maintain the radar performance and reduce the RCS of an antenna array [26]. However, the reported topology has difficulties in attaining polarization stability due to the additional bias lines for active elements. Although a polarization-insensitive switchable design that acts as a radar absorber or a transmission screen under different states of PIN diodes is presented in [27], the issue of narrow reconfigurable bandwidth still requires resolution. Besides, the insertion loss, device cost and high-frequency applicability introduced by the active elements should also be thoroughly considered.

In addition, the vast majority of FSS absorbers merely focus on microwave absorbing properties, while the features in the visible and infrared spectral regions are also worth exploring for the application requirements of multispectral camouflage. While there have been advancements in developing combined radar-infrared stealth structures [28], [29], [30], few designs have achieved compatibility across radar, visible light, and infrared spectra. Furthermore, these designs have also faced challenges in incorporating reconfigurability and controllability features. Therefore, a simple configuration of wideband and dual-polarized reconfigurable absorber, which can switch between two opposite states of absorption and transmission at microwave band while integrating multispectral regulation capability in the visible and infrared spectra, has yet to be realized.

In this paper, an absorption/transmission switchable frequency selective surface (A/T-SFSS) with wideband and polarization-insensitivity characteristics is proposed. A groundless absorber, consisting of structured water encapsulated by a polydimethylsiloxane (PDMS) container, is designed as the top absorbing layer at first. The water-based structure exhibits wideband and efficient radar absorbing ability when filled with pure water. Then, a second-order bandpass FSS structure with high selectivity is arranged below the water-based element. Once the pure water inside the PDMS container is discharged, a center passband with flat top properties and two transmission zeros distributed at both sides can be obtained. By manipulating the status of liquid injection, an obvious wideband switching function between absorption and transmission states can be obtained, and the overall performance of the two opposite operating states is well balanced. Compared to the switchable absorption/transmission screens aforementioned, the proposed design simultaneously possesses advantages in the aspects of wide switchable bandwidth, high passband selectivity and good stability with respect to different polarizations and incident angles. Furthermore, for the first time in the literature to the best of the authors' knowledge, one unique feature is achieved, consisting in the adaptability of the A/T-SFSS in both visible and infrared wavelengths. With its simultaneous capabilities of visible light camouflage and infrared radiation regulation, the developed A/T-SFSS finds practical applications in military operations, surveillance systems, and wildlife conservation. These technologies enhance stealth, situational awareness, and observational capabilities, contributing to improved effectiveness and security in a wide range of applications. Finally, the corresponding results demonstrate its potential in the multispectral compatible camouflage domain.

II. DESIGN AND ANALYSIS OF THE A/T-SFSS

The schematic diagram of the A/T-SFSS array is illustrated in Fig. 1(a). The proposed structure is composed of a wideband water-based absorber (WWA) and a second-order bandpass FSS with high selectivity. As depicted in Fig. 1(b), the unit cell of the upper structured water, consisting of a cross microfluidic channel and a cylindrical resonator, is encapsulated by a PDMS container ($\varepsilon_0 = 2.72$, $\tan\delta_0 = 0.0027$). Taking the advantage of its flowability, the water medium inside the container can be connected and circulated through the cross microfluidic channel. The lower

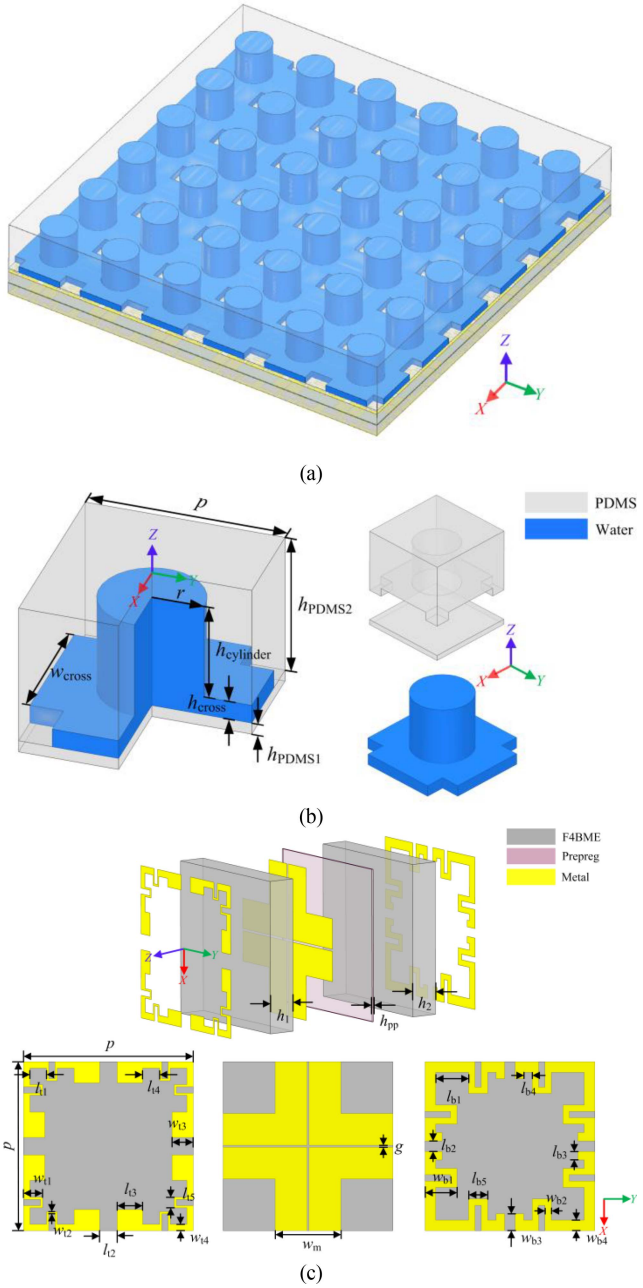

FIGURE 1. The schematic diagram of the proposed design. (a) The A/T-SFSS array. (b) The upper water-based absorbing structure. (c) The lower second-order bandpass structure.

transmission layer in Fig. 1(c) is realized by a second-order bandpass topology with three metallic structures supported by two F4BME dielectric layers ($\varepsilon_1 = 2.85$, $\tan\delta_1 = 0.0007$), which are bonded by a FR4 prepreg layer ($\varepsilon_2 = 4.4$, $\tan\delta_2 = 0.02$). With reference to Fig. 1(c), the values of the geometric parameters are as follow: $p = 8$ mm, $l_{t1} = 0.735$ mm, $l_{t2} = 0.83$ mm, $l_{t3} = 1.2$ mm, $l_{t4} = 0.8$ mm, $l_{t5} = 0.5$ mm, $w_{t1} = 0.9$ mm, $w_{t2} = 0.1$ mm, $w_{t3} = 0.8$ mm, $w_{t4} = 0.35$ mm, $w_m = 3.3$ mm, $g = 0.12$ mm, $l_{b1} = 1.65$ mm, $l_{b2} = 0.5$ mm, $l_{b3} = 0.35$ mm, $l_{b4} = 0.35$ mm, $l_{b5} = 0.9$ mm, $w_{b3} = 0.7$ mm, $w_{b1} = 1.5$ mm, $w_{b2} = 0.3$ mm, $w_{b4} = 0.5$ mm, $w_{cross} = 5.3$ mm, $r = 2.1$ mm, $h_{cross} = 0.8$ mm, $h_{cylinder} = 4.9$ mm, $h_{PDMS1} = 0.5$ mm, $h_{PDMS2} = 6$ mm, $h_{pp} = 0.08$ mm, and $h_1 = h_2 = 1.43$ mm.

A. SWITCHABLE MICROWAVE PERFORMANCE

Two independent EM states of absorption and transmission can be achieved by controlling the injection condition of pure water. The A/T-SFSS operates as a dual-polarized wideband absorber when the container is full of pure water; contrarily, the A/T-SFSS features bandpass filtering characteristics with high selectivity and polarization insensitivity when pure water is drained out. For further numerical analyses, the EM simulation software HFSS based on the finite element method (FEM) is adopted. Two Floquet ports are applied along z axis as the excitation, and two pairs of periodic boundaries are assigned in both x and y directions to mimic the periodic array by analyzing only one unit cell.

1) WIDEBAND ABSORPTION STATE

In order to achieve wideband absorbing properties of the A/T-SFSS, pure water is used as the dispersive and lossy medium inside the container. The complex permittivity of pure water at room temperature of 25 °C is first studied and it can be described by using the first-order Debye model [31]:

$$\varepsilon(\omega, T_{pw}) = \varepsilon_\infty(T_{pw}) + \frac{\varepsilon_0(T_{pw}) - \varepsilon_\infty(T_{pw})}{1 - i\omega\tau(T_{pw})} \quad (1)$$

where ω and T_{pw} are the frequency and water temperature. The parameters ε_0, ε_∞ and τ are the static permittivity, optical permittivity and rotational relaxation time, respectively. These temperature-related parameters can be approximated by the following polynomial functions:

$$\varepsilon_0(T_{pw}) = a_1 - b_1 T_{pw} + c_1 {T_{pw}}^2 - d_1 {T_{pw}}^3 \quad (2)$$

$$\varepsilon_\infty(T_{pw}) = \varepsilon_0(T_{pw}) - a_2 e^{-b_2 T_{pw}} \quad (3)$$

$$\tau(T_{pw}) = c_2 e^{T_2/(T_{pw}+T_1)} \quad (4)$$

where $a_1 = 87.9$, $b_1 = 0.404$ K^{-1}, $c_1 = 9.59\times10^{-4}$ K^{-2}, $d_1 = 1.33\times10^{-6}$ K^{-3}, $a_2 = 80.7$, $b_2 = 4.42\times10^{-3}$ K^{-1}, $c_2 = 1.37\times10^{-13}$ s, $T_1 = 133$ °C, and $T_2 = 651$ °C.

Then, the calculated frequency-dependent dielectric constant and loss tangent of pure water are imported into the simulation software. The absorptivity $A(\omega)$ can be defined as:

$$A(\omega) = 1 - |T(\omega)| - |R(\omega)| = 1 - |{S_{21}}^2(\omega)| - |{S_{11}}^2(\omega)| \quad (5)$$

where $T(\omega)$ and $R(\omega)$ are the transmissivity and reflectivity, respectively, while $S_{21}(\omega)$ and $S_{11}(\omega)$ are the transmission and reflection coefficients, respectively.

The simulated absorption curves of the proposed A/T-SFSS under normal incidence are depicted in Fig. 2(a). The structure exhibits wideband absorbing characteristics, with an absorbing bandwidth of 6.50 - 10.48 GHz and an absorbing rate exceeding 0.9, resulting in a fractional bandwidth of

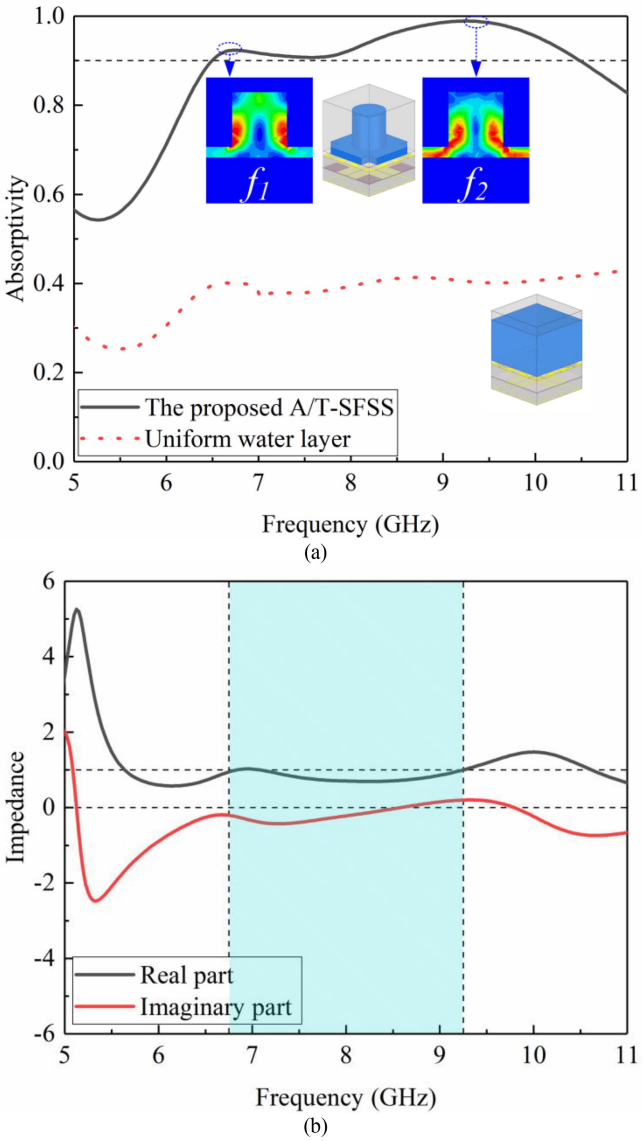

FIGURE 2. (a) The simulated absorption curves of the proposed A/T-SFSS and the uniform water layer. (b) The normalized impedance of the A/T-SFSS.

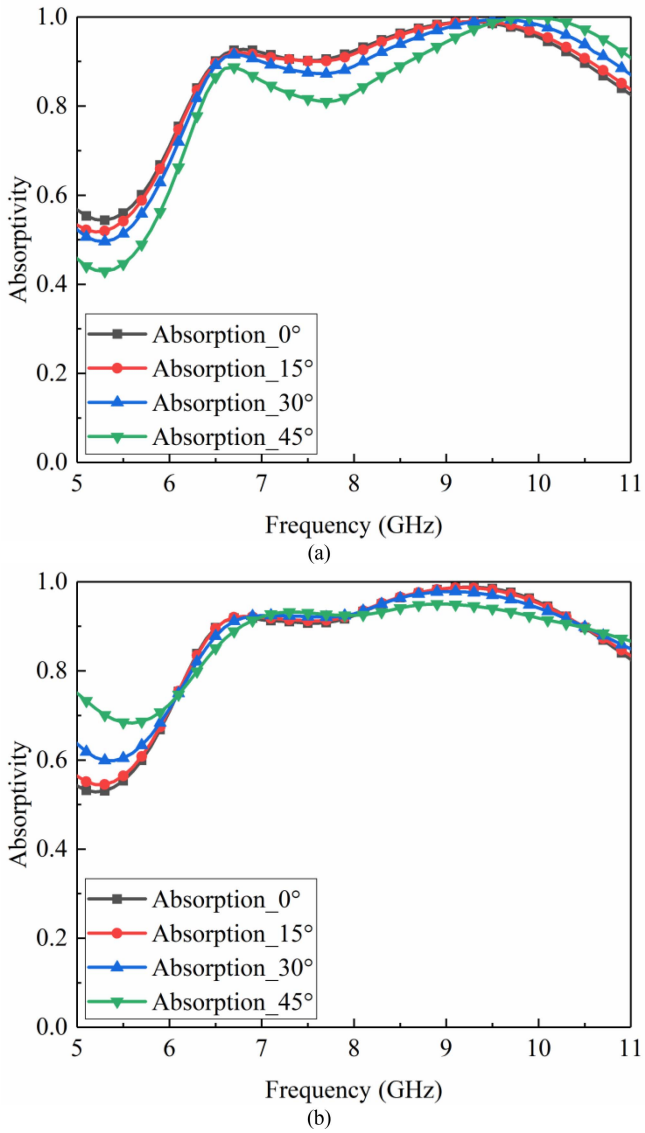

FIGURE 3. The simulated absorption curves of the proposed A/T-SFSS under oblique incidence. (a) TE polarization. (b) TM polarization.

about 46.9% at absorption state. Besides, the absorptivity of a layer of uniform water with the same thickness is also compared with that of the A/T-SFSS, indicating the contribution of structured water to the wideband absorption.

To attain further insights into the absorbing mechanism of the A/T-SFSS, the distributions of loss density in the *yoz* plane at the two absorption peaks of $f_1 = 6.75$ GHz and $f_2 = 9.25$ GHz are added as insets in Fig. 2(a). It can be observed that the losses mainly concentrate inside the structured water instead of the PDMS container within the operating band due to the large dielectric losses of pure water. At 6.75 GHz, the power losses mainly dissipate in the places where the cylindrical resonator are in contact with the PDMS shell side, whilst the power losses are also generated at the two sides of the cross water structure adjacent to the bottom PDMS coating at 9.25 GHz. Hence, it is the synergetic effect of these different resonant modes that contributes to the expansion of the absorbing bandwidth.

The normalized impedance $Z_{\mathrm{ni}}(\omega)$ of the A/T-SFSS can be extracted according to (6). As plotted in Fig. 2(b), it can be seen that the real part of the normalized impedance is close to 1 while the imaginary part is close to 0 from 6.50 GHz to 10.48 GHz, which indicates that the impedance matching condition is well satisfied within the entire absorbing band.

$$Z_{\mathrm{ni}}(\omega) = \pm\sqrt{\frac{(1+S_{11}(\omega))^2 - S_{21}(\omega)}{(1-S_{11}(\omega))^2 + S_{21}(\omega)}} \tag{6}$$

The simulated absorption rates of the A/T-SFSS under different incident angles and polarizations are further studied and plotted in Fig. 3, and the absorptivity maintains high levels even when the incident angle increases up to 45°. However, the absorptivity exhibits relatively better

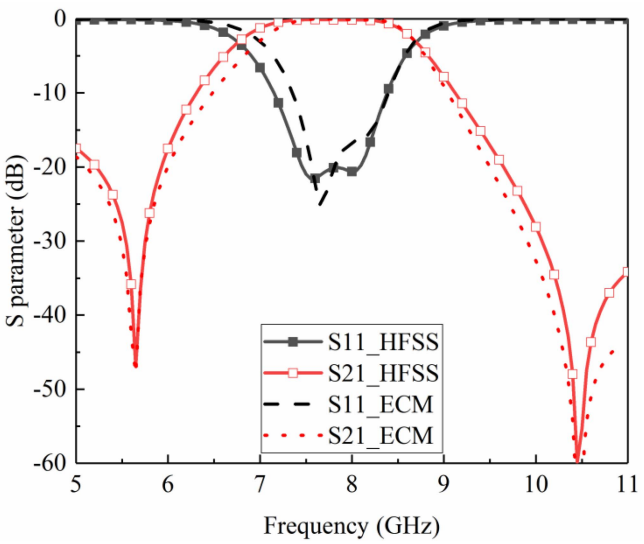

FIGURE 4. The simulated and calculated scattering curves of the proposed A/T-SFSS at transmission state.

angle stability for TM polarization (the electric field is oriented along the *x*-axis direction) than TE polarization (the electric field is oriented along the *y*-axis direction). This phenomenon can be explained by the weaker magnetic component of the TE-polarized waves as the incident angle increases, which deteriorates the effect of dielectric resonance [32].

2) HIGHLY-SELECTIVE TRANSMISSION STATE

When pure water is discharged from the PDMS container, the wideband absorption state can be switched to the entirely opposite transmission state with high selectivity. The simulated scattering coefficients of the A/T-SFSS at transmission state under normal incidence are shown in Fig. 4. The −1 dB and −3 dB transmission bandwidths are 1.43 GHz (7.04 - 8.47 GHz) and 1.91 GHz (6.78 - 8.69 GHz), respectively, and the minimum insertion loss at the transmission band is only 0.1 dB. Besides, the feature of good selectivity is guaranteed with two transmission zeros distributed at both sides of the center transmission band. By employing symmetrical meander-line structures coupled with a nonresonant inductive wire grid in the transmission layer, two transmission poles and one transmission zero above the passband can be generated within the operating band. Moreover, the introduction of capacitive gaps in the middle-layer structure allows for the generation of an additional transmission zero below the passband, with its position adjustable by modifying the geometric parameters of the grid and gap structures.

Based on the transmission line theory, the equivalent circuit model (ECM) of the A/T-SFSS is established. As shown in Fig. 5, the metallic structures from top to down can be modeled as the series resonant circuits L_tC_t, L_mC_m and L_bC_b, respectively. The two supporting substrates in between can be represented by the hybrid circuits $L_{s1}C_{s1}$

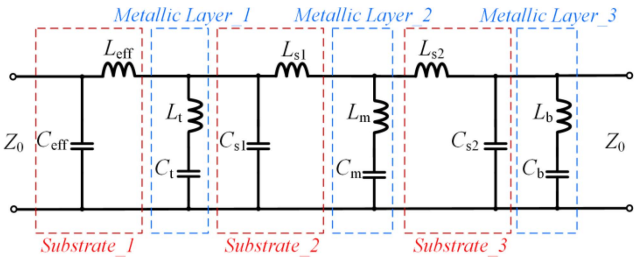

FIGURE 5. The equivalent circuit model of the proposed A/T-SFSS.

and $L_{s2}C_{s2}$, respectively. The hollow PDMS container is converted to an equivalent homogeneous dielectric layer with the same thickness, whose effective permittivity can be calculated by using the volume-weighted average method. After that, the uniform substrate can be equivalent to the lumped components $L_{eff}C_{eff}$. The bonding layer can be neglected in the circuit calculation since its thickness is very thin. The equivalent circuit parameters mentioned above are first calculated according to the approximation formulas given in [33], [34], and then they are set as the initial values in the Advanced Design System (ADS) software before the curve fitting procedure. The final optimized circuit parameters are listed as follow: $L_t = 2.932$ nH, $C_t = 0.079$ pF, $L_m = 1.810$ nH, $C_m = 0.441$ pF, $L_b = 2.272$ nH, $C_b = 0.077$ pF, $L_{eff} = 6.734$ nH, $C_{eff} = 0.039$ pF, $L_{s1} = L_{s2} = 1.692$ nH, and $C_{s1} = C_{s2} = 0.034$ pF. The calculated transmission and reflection coefficients are compared in Fig. 4, which are in good agreement with the simulated ones.

The circumstances of oblique incidence at transmission state are presented in Fig. 6. The in-band transmission characteristics of the proposed design hold stable as the incident angle increases up to 45°. The transmission bandwidth gradually increases at TE polarization, which is contrary to the variation rule at TM polarization.

3) MICROWAVE PERFORMANCE VALIDATION

In order to validate the microwave performance of the proposed design, an A/T-SFSS prototype with an overall dimension of 150 mm × 150 mm is fabricated and measured in an anechoic chamber. As shown in Fig. 7(a), the upper and lower structures are assembled together by employing nylon columns and nuts at the edges and corners. Pure water is injected into microfluidic channels through the inlet/outlet located on the outer side of the prototype. The interconnected structure of neighboring units allows for the use of a single pair of inlet and outlet. For convenience, a syringe is used for the injection of pure water in the experiment. Two small openings along the diagonal, connecting to the syringe through PTFE tubes and hollow steel needles, are drilled in the microscale machining process for the injection and discharge of pure water. To further improve the control efficiency and stability at a constant speed, a micropump can be considered in practical operations. The measurement settings of reflection (left) and transmission (right) coefficients are

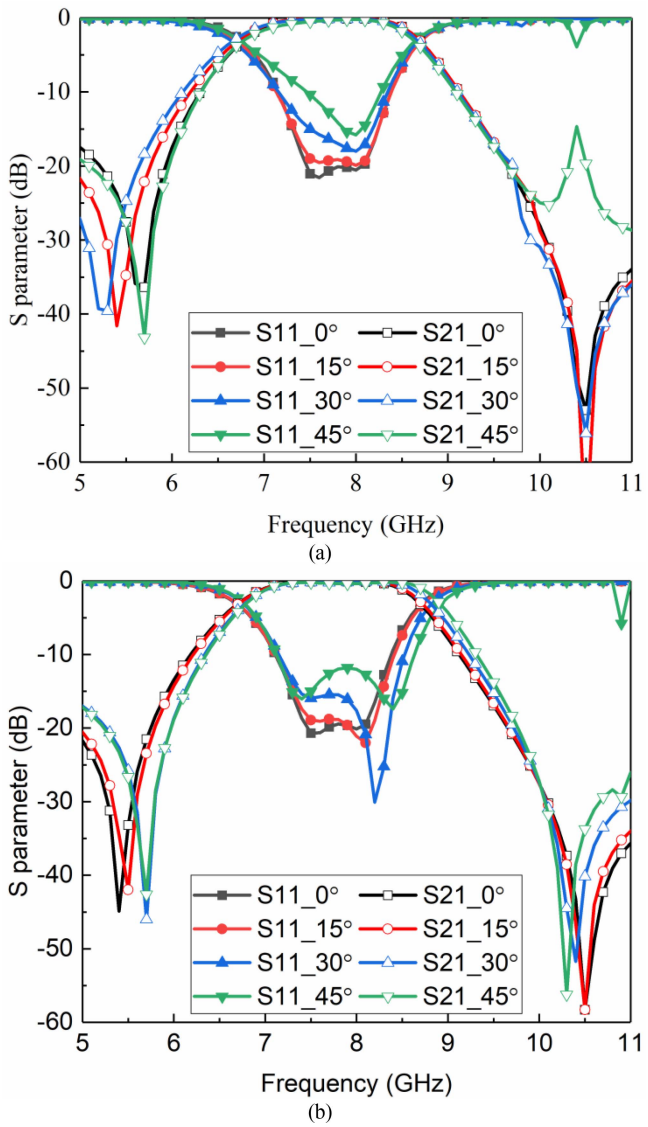

FIGURE 6. The simulated scattering curves of the proposed A/T-SFSS under oblique incidence. (a) TE polarization. (b) TM polarization.

shown in Fig. 7(b). A pair of horn antennas (2 - 18 GHz) from Guanjun Technology, which acts as the transmitting and receiving antennas, is connected to the two ports of an Agilent vector network analyzer (VNA) N5245A. The time-domain gating technique is adopted during the test to reduce the interferences of system noise. The transmission and reflection coefficients should be measured separately. For the reflection test, two antennas are set at the same side of a foam window with the size of 600 mm × 600 mm, and the fabricated sample is arranged at the center. The reflection coefficients are calculated by normalizing the measured results to those of a metallic sheet with the same size. To attain transmission coefficients, two antennas are placed at both sides of an equally-sized foam window but with conductive copper tapes attached to the surface. The measured data of the air are then used as the reference

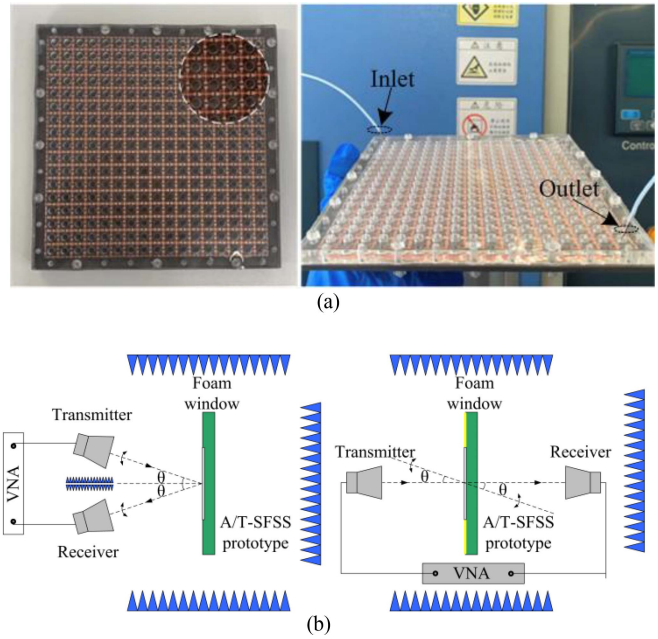

FIGURE 7. (a) The fabricated prototype of the proposed A/T-SFSS. (b) The measurement setups of microwave scattering parameters.

background to obtain the transmission coefficients of the prototype.

The experimental results of the proposed A/T-SFSS at both absorption and transmission states are provided in Fig. 8. From the absorbing curves given in Fig. 8(a) and Fig. 8(b), it can be seen that the wideband absorbing capability of the A/T-SFSS is well maintained, although the measured absorption rates are marginally lowered because of the air bubbles introduced during liquid injection. As shown in Fig. 8(c) and Fig. 8(d), the A/T-SFSS features the transmission properties of flat top and high selectivity under normal incidence. The out-of-band curves slightly rise, which can be explained by the edge diffraction effect of the limited-sized prototype. In addition, the A/T-SFSS is also demonstrated to be polarization-insensitive and exhibits stable responses as the incident angle increases to 45° at different states.

B. VISIBLE LIGHT CAMOUFLAGE

By pumping colored solutions into the microchannel structure, the differences between the proposed A/T-SFSS and the background can be adjusted in the visible spectrum. The soluble gouache paints are chosen as the colorants and diluted in water to obtain colored solutions. Although various colored solutions can be prepared, the gray colored solution is used as the sample of the following experiment considering that the gray slate is easily available near the college.

To present the camouflage performance of the A/T-SFSS in visible light, an image analysis program is developed. First of all, the images of the A/T-SFSS with and without camouflaging coloration are taken on a slate background.

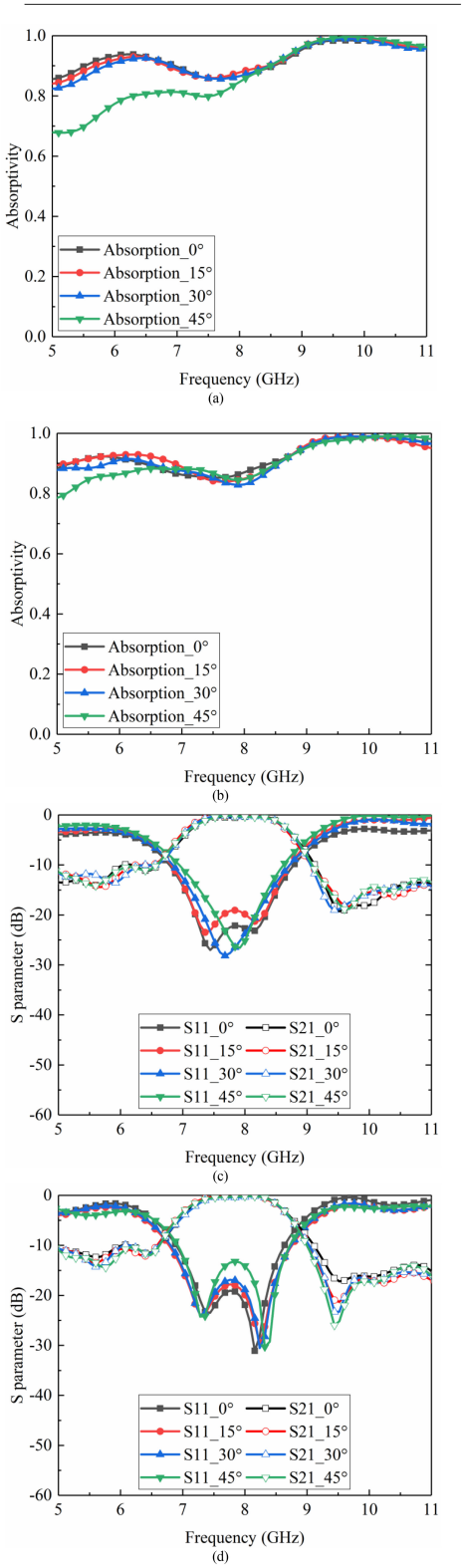

FIGURE 8. The measured results of the proposed A/T-SFSS. (a) The absorption state at TE polarization. (b) The absorption state at TM polarization. (c) The transmission state at TE polarization. (d) The transmission state at TM polarization.

After that, the collected images are converted to 8 bit grayscale, whose color intensity ranges from 0 (black color) to 255 (white color). The quantitative information about the

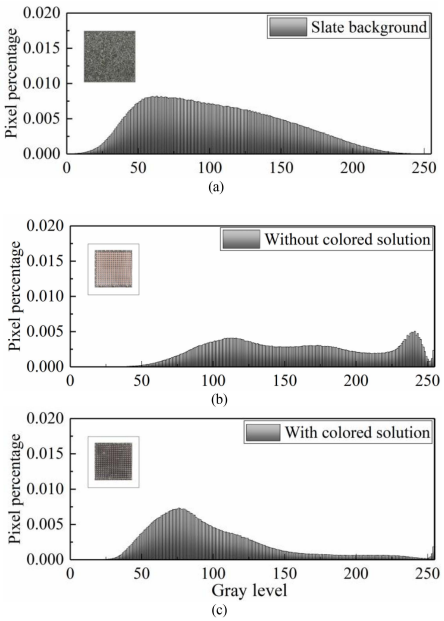

FIGURE 9. The normalized gray histograms. (a) The slate background. (b) The proposed A/T-SFSS without camouflaging coloration. (c) The proposed A/T-SFSS with camouflaging coloration.

brightness and contrast characteristics can be obtained by (7) and (8):

$$\mu_I = \frac{1}{N}\sum I(x, y) \tag{7}$$

$$\sigma_I = \sqrt{\frac{1}{N}\sum (I(x, y) - \mu_{\mathrm{I}})^2} \tag{8}$$

where μ_{I} is the mean brightness and σ_I is the root mean square contrast. N is the total number of pixels in the image and $I(x, y)$ represents brightness value of the pixel at coordinates (x, y).

The calculated $(\mu_{\mathrm{I}}, \sigma_I)$ values of the slate background and the A/T-SFSS with and without camouflaging coloration are (103.89, 46.11), (103.50, 46.36) and (137.72, 56.15), respectively, indicating that the brightness and contrast of the camouflaged A/T-SFSS are much closer to that of the slate background.

In order to show the camouflage effectiveness more intuitively, the normalized grayscale histograms of the brightness is further provided. The image regions containing the A/T-SFSS are firstly extracted and isolated from the background. Then, the normalized grayscale histograms of the slate background and the A/T-SFSS under different situations are plotted in Fig. 9 with the analyzed images added as insets. This visualization of the gray histogram intuitively demonstrates the feasibility of the camouflaging coloration approach.

However, the complex permittivity of the colored solution is different from that of pure water, which will inevitably impact the absorption capability of the A/T-SFSS in the microwave band. Thus, a precise knowledge of the complex

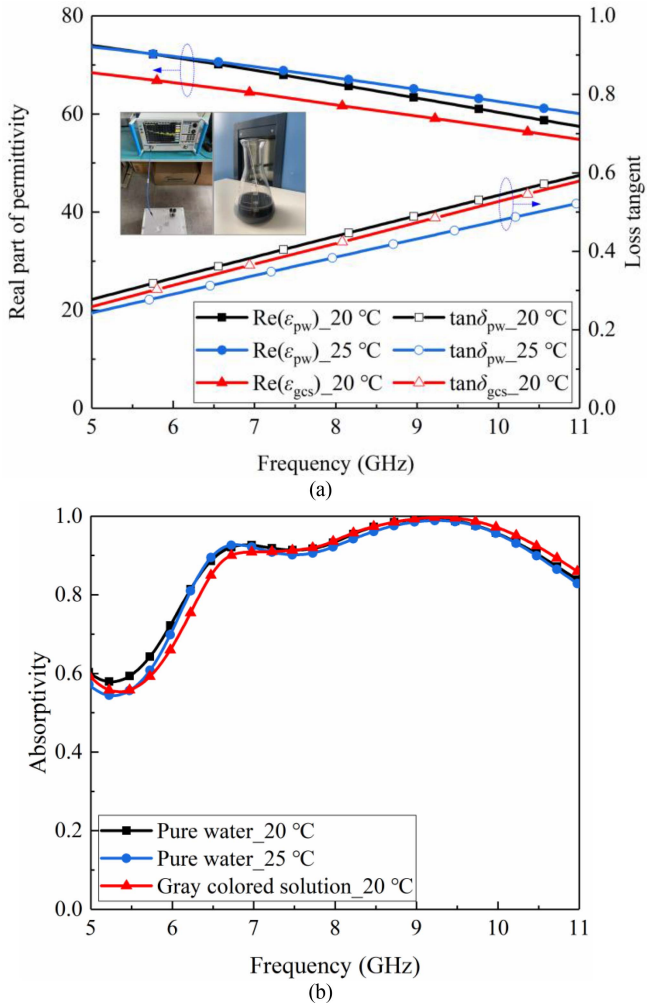

FIGURE 10. (a) The EM parameters of the gray colored solution and pure water. (b) The compared absorbing curves of the A/T-SFSS with gray colored solution and pure water.

permittivity data of colored fluid dielectric materials should be attained before they can be used for the intended EM applications. In this paper, accurate measurements of the EM parameters of such water-based liquids are performed by the coaxial probe method, and the measurement setup is added as an inset in Fig. 10. The coaxial probe is connected to the Ceyear VNA 3671G by the test cable with stable amplitude and phase characteristics. In order to remove systematic errors of measurements, single port calibrations of three standards including terminal open circuit, terminal short circuit, and deionized water are required before each actual test.

The real part of the dielectric constant and the loss tangent of the gray colored solution are measured (20 °C) and compared with those of pure water (20 °C and 25 °C) in Fig. 10(a), where [Re(ε_{pw}), tanδ_{pw}] and [Re(ε_{gcs}), tanδ_{gcs}] denote the EM parameters of pure water and gray colored solution, respectively. The tested dielectric parameters of the colored solution are then imported into the simulation software to investigate their influence on the microwave

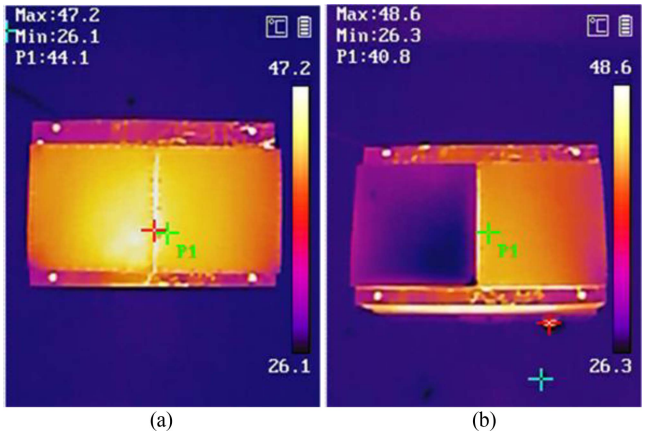

FIGURE 11. The compared infrared radiation images of the proposed A/T-SFSS with and without pure water. (a) Both samples are heated at 50 °C for more than 10 minutes. (b) The water temperature of the left sample is changed to 18.5 °C through water circulation.

absorbing performance of the A/T-SFSS. As shown in Fig. 10(b), although subtle differences can be observed, the absorbing characteristics maintain well after pure water is replaced by the colored solution.

C. INFRARED RADIATION REGULATION

According to the Stefan-Boltzmann's law, the infrared radiation of an object can be described by the following formula:

$$M = \varepsilon(T)\sigma T^4 \tag{9}$$

where M is the infrared radiation, $\sigma \approx 5.67 \times 10^{-8}$ W/(m^2·K^4) is the Stefan-Boltzmann constant, T and $\varepsilon(T)$ are the temperature and infrared emissivity, respectively. It is clear that the infrared radiation is proportional to both temperature and emissivity of the object itself. For the proposed water-based structure, the infrared radiation can be controlled by changing the temperature of the injected pure water considering the large heat capacity of pure water.

To demonstrate its capability in regulating the infrared radiation, two prototypes of the A/T-SFSS with and without pure water are placed on the left and right sides of a heating table with an ambient temperature around 25 °C. The thermal imager HM-TPH11-3AXF from HIKMICRO is utilized to record the infrared radiations. As shown in Fig. 11(a), the two samples show similar infrared radiation characteristics after being heated at the working temperature of 50 °C for more than 10 minutes. Then, it can be obviously observed in Fig. 11(b) that the sample on the left exhibits much weaker infrared radiations after another round of water circulation with a lower temperature of 18.5 °C. Therefore, the infrared radiation features can be easily manipulated by dynamically regulating the temperature of circulating water.

As the complex permittivity of pure water is temperature-dependent, it is necessary to study the effect of temperature variation on the microwave absorbing properties at absorption state. As shown in Fig. 12, the absorption intensity and bandwidth are gradually narrowed as the water temperature

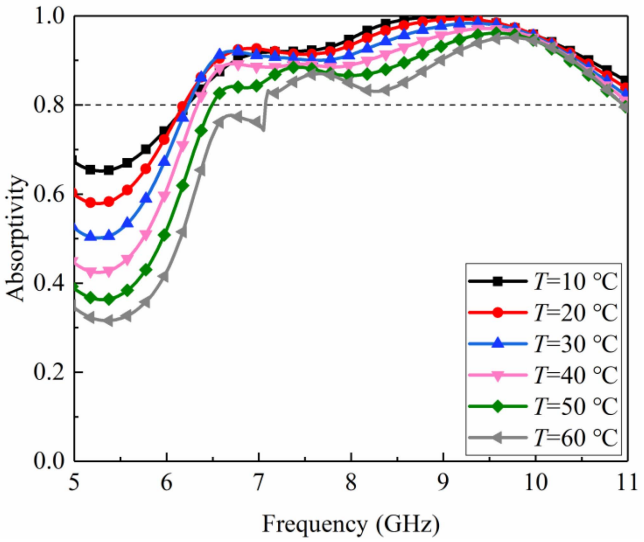

FIGURE 12. The absorption spectra of the proposed A/T-SFSS under different temperatures of pure water.

TABLE 1. Comparison between the proposed design and previously reported literatures.

Design	AB[a1](GHz) FBW[a2]	TB[b1](GHz) IL[b2](dB)	PI[c]	AS[d]	VIS[e]	IR[f]
[26][#]	8.65-9.74 11.9%	8-9.34 0.16	No	Not given	/	/
[27][#]	Narrowband	Narrowband 0.96	Yes	60°	/	/
[28]	Narrowband	/	Yes	45°	/	LIR[f1]
[29]	5.1-19.2 116%	/	Yes	45°	VLT[e1]	LIR[f1]
[30]	7.7-18 80.2%	/	Yes	40°	VLT[e1]	LIR[f1]
This paper[#]	6.5-10.48 46.9%	7.04-8.47 0.1	Yes	45°	VLC[e2]	IRR[f2]

[a1]Microwave absorbing band with an absorptivity greater than 0.9 and [a2]its fractional bandwidth; [b1]microwave transmission band above -1 dB and [b2]minimum insertion loss of passband; [c]polarization insensitivity; [d]angle stability; [e]visible light, [e1]visible light transparent, [e2]visible light camouflage; [f]infrared, [f1]low infrared emissivity, [f2]infrared radiation regulation; [#]designs with switchable absorption/transmission capabilities.

increases. The variation in the lower frequency band is relatively larger than that at the higher frequencies. In spite of the change in absorption spectra, the absorption intensities within the band of interest remain larger than 80% even when the temperature increases up to 60 °C.

A comprehensive comparison has been provided in Table 1 to demonstrate the superiorities of the proposed structure in relation to previous designs. The table highlights critical parameters such as microwave absorption/transmission bandwidth, passband insertion loss, polarization insensitivity, angle stability, and characteristics in the visible light and infrared spectra. Compared to the aforementioned studies, the proposed design in this paper is a multifunctional and multispectral solution that combines the advantages of wideband switchable microwave absorption/transmission states with active control over visible light and infrared spectra. This integration positions the proposed design as highly promising for extensive applications in the field of multispectral stealth.

III. CONCLUSION

A wideband and dual-polarized A/T-SFSS, characterized by multispectral characteristics, is proposed and studied in this paper. By controlling the accurately designed water structure in microfluidic channels, a wideband and efficient modulation of absorption and transmission performance at microwaves can be realized with good angle stability. Furthermore, the simultaneous functions of visible light camouflage and infrared radiation management of the A/T-SFSS are also studied by changing the color and temperature of the water medium inside microfluidic channels. For demonstration, a prototype is fabricated and then the experiments in microwave, visible light and infrared regions are conducted separately to validate its multispectral features. The proposed A/T-SFSS serves as the first step towards integrating more operating capabilities of spectra tailoring, and it can be a potential candidate for various fields such as the multispectral compatible camouflage and communication systems. The presence of liquid provides a high degree of flexibility since its properties can be matched to derive more challenging multispectral configurations. However, it should be noted that despite the demonstrated potential in theoretical and experimental research, practical applications of water-based reconfigurable FSS still face challenges such as fabrication, stability, and cost considerations, which necessitates further research and development to drive its widespread adoption across various fields.

ACKNOWLEDGMENT

The authors thank the engineers F. Zhang and C. Chen from Ceyear Technologies Co., Ltd for their help in measuring EM parameters of colored solutions.

REFERENCES

[1] M. Zargar, A. Rajput, K. Saurav, and S. Koul, "Frequency-selective rasorber based on high-Q minkowski fractal-shaped resonator for realizing a low radar cross-section radiating system," *IEEE Trans. Electromagn. Compat.*, vol. 64, no. 5, pp. 1574–1584, Oct. 2022.

[2] M. Shukoor, S. Dey, and S. Koul, "A simple polarization-insensitive and wide angular stable circular ring based undeca-band absorber for EMI/EMC applications," *IEEE Trans. Electromagn. Compat.*, vol. 63, no. 4, pp. 1025–1034, Aug. 2021.

[3] F. Erkmen and O. Ramahi, "A scalable, dual-band absorber surface for electromagnetic energy harvesting and wireless power transfer," *IEEE Trans. Antennas Propag.*, vol. 69, no. 10, pp. 6982–6987, Oct. 2021.

[4] X. Lv, S. Chen, A. Galehdar, W. Withayachumnankul, and C. Fumeaux, "Fast semi-analytical design for single-FSS-layer circuit-analog absorbers," *IEEE Open J. Antennas Propag.*, vol. 1, pp. 483–492, 2020.

[5] Z. Yao, S. Xiao, Y. Li, and B. Wang, "On the design of wideband absorber based on multilayer and multiresonant fss array," *IEEE Antennas Wireless Propag. Lett.*, vol. 20, no. 3, pp. 284–288, Mar. 2021.

[6] A. Parameswaran, A. Ovhal, D. Kundu, H. Sonalikar, J. Singh, and D. Singh, "A low-profile ultra-wideband absorber using lumped resistor-loaded cross dipoles with resonant nodes," *IEEE Trans. Electromagn. Compat.*, vol. 64, no. 5, pp. 1758–1766, Oct. 2022.

[7] Y. Yoo et al., "Metamaterial absorber for electromagnetic waves in periodic water droplets," *Sci. Rep.*, vol. 5, no. 1, 2015, Art. no. 14018.
[8] X. Huang, H. Yang, Z. Shen, J. Chen, H. Lin, and Z. Yu, "Water-injected all-dielectric ultra-wideband and prominent oblique incidence metamaterial absorber in microwave regime," *Appl. Phys.*, vol. 50, no. 38, 2017, Art. no. 385304.
[9] Z. Shen et al., "An ultra-wideband, polarization insensitive, and wide incident angle absorber based on an irregular metamaterial structure with layers of water," *Appl. Phys.*, vol. 123, no. 22, 2018, Art. no. 225106.
[10] J. Ren and J. Yin, "Cylindrical-water-resonator-based ultra-broadband microwave absorber," *Opt. Mater. Exp.*, vol. 8, no. 8, pp. 2060–2071, 2018.
[11] X. Zhang et al., "3-D printed swastika-shaped ultrabroadband water-based microwave absorber," *IEEE Antennas Wireless Propag. Lett.*, vol. 19, no. 5, pp. 821–825, May 2020.
[12] X. Zhang, F. Yan, X. Du, W. Wang, and M. Zhang, "Broadband water-based metamaterial absorber with wide angle and thermal stability," *AIP Adv.*, vol. 10, no. 5, 2020, Art. no. 55211.
[13] Y. Chen et al., "Ultrabroadband microwave absorber based on 3D water microchannels," *Photon. Res.*, vol. 9, no. 7, pp. 1391–1396, 2021.
[14] J. Wen et al., "Progress in water-based metamaterial absorbers: A review," *Opt. Mater. Exp.*, vol. 12, no. 4, pp. 1461–1479, 2022.
[15] S. Li et al., "Multifunctional water-based metamaterial with polarization conversion and absorption," *Opt. Exp.*, vol. 31, no. 2, pp. 3336–3348, 2023.
[16] M. Odit, P. Kapitanova, A. Andryieuski, P. Belov, and A. Lavrinenko, "Experimental demonstration of water based tunable metasurface," *Appl. Phys. Lett.*, vol. 109, no. 1, 2016, Art. no. 11901.
[17] J. Ge, Y. Zhang, H. Li, H. Dong, and L. Zhang, "Ultra-broadband, tunable, and transparent microwave meta-absorber using ITO and water substrate," *Adv. Opt. Mater.*, vol. 11, no. 10, 2023, Art. no. 2202873.
[18] Y. Zhang, H. Dong, N. Mou, H. Li, X. Yao, and L. Zhang, "Tunable and transparent broadband metamaterial absorber with water-based substrate for optical window applications," *Nanoscale*, vol. 13, no. 20, pp. 7831–7837, 2021.
[19] H. Jeong, E. Park, and S. Lim, "Three-dimensional printed and fluidic dielectric material optically transparent metasurface for switchable absorption and reflection functionality in microwave frequency region," in *Waves in Random and Complex Media*. London, U.K.: Informa, 2022. [Online]. Available: https://doi.org/10.1080/17455030.2022.2058712
[20] H. Li et al., "Transparent and broadband switchable absorber/reflector based on structured water medium," *J. Phys. D Appl. Phys.*, vol. 55, no. 43, 2022, Art. no. 435005.
[21] Y. Shang, Z. Shen, and S. Xiao, "Frequency-selective rasorber based on square-loop and cross-dipole arrays," *IEEE Trans. Antennas Propag.*, vol. 62, no. 11, pp. 5581–5589, Nov. 2014.
[22] Q. Chen, D. Sang, M. Guo, and Y. Fu, "Frequency-selective rasorber with interabsorption band transparent window and interdigital resonator," *IEEE Trans. Antennas Propag.*, vol. 66, no. 8, pp. 4105–4114, Aug. 2018.
[23] Q. Chen, D. Sang, M. Guo, and Y. Fu, "Miniaturized frequency-selective rasorber with a wide transmission band using circular spiral resonator," *IEEE Trans. Antennas Propag.*, vol. 67, no. 2, pp. 1045–1052, Feb. 2019.
[24] Y. Han, W. Che, X. Xiu, W. Yang, and C. Christopoulos, "Switchable low-profile broadband frequency-selective rasorber/absorber based on slot arrays," *IEEE Trans. Antennas Propag.*, vol. 65, no. 12, pp. 6998–7008, Dec. 2017.
[25] R. Dutta, J. Ghosh, and A. Sarkhe, "Planar frequency selective surface-based switchable rasorber/absorber for airborne application," *IEEE Antennas Wireless Propag. Lett.*, vol. 21, no. 9, pp. 1842–1846, Sep. 2022.
[26] S. Kitagawa, S. Ryosuke, H. Osamu, and A. Kiyomichi, "Study on RCS reduction of patch array using switchable absorption/transmission surface," *IEICE Trans. Electron.*, vol. E99.C, no. 7, pp. 805–808, 2016.
[27] P. Sainadh, A. Sharma, and S. Ghosh, "Polarization-insensitive absorptive/transmissive reconfigurable frequency selective surface with embedded biasing," *IEEE Antennas Wireless Propag. Lett.*, vol. 22, no. 1, pp. 164–168, Jan. 2023.
[28] C. Xu et al., "Hybrid metasurfaces for infrared-multiband radar stealth-compatible materials applications," *IEEE Access*, vol. 7, pp. 147586–147595, 2019.
[29] C. Yang et al., "Thermal infrared and broadband microwave stealth glass windows based on multi-band optimization," *Opt. Exp.*, vol. 29, no. 9, pp. 13610–13623, 2021.
[30] C. Zhang et al., "Flexible and transparent microwave-infrared bistealth structure," *Adv. Mat. Technol.*, vol. 4, no. 8, 2019, Art. no. 1900063.
[31] W. Ellison, "Permittivity of pure water, at standard atmospheric pressure, over the frequency range 0–25 THz and the temperature range 0–100 °C," *J. Phys. Chem. Ref. Data*, vol. 36, no. 1, pp. 1–18, 2007.
[32] X. Liu, K. Bi, B. Li, Q. Zhao, and J. Zhou, "Metamaterial perfect absorber based on artificial dielectric "atoms,""*Opt. Exp.*, vol. 24, no. 18, pp. 20454–20460, 2016.
[33] F. Bayatpur, "Metamaterial-inspired frequency-selective surfaces," Ph.D. dissertation, Dept. Electr. Eng., Univ. Michigan, Ann Arbor, MI, USA, 2009.
[34] F. Costa, A. Monorchio, and G. Manara, "An overview of equivalent circuit modeling techniques of frequency selective surfaces and metasurfaces," *Appl. Comput. Electromagn. Soc. J.*, vol. 29, no. 12, pp. 960–976, 2014.

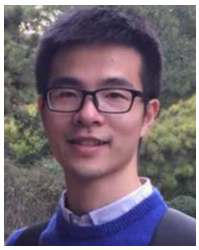

HUANGYAN LI (Member, IEEE) received the B.E. and M.E. degrees from the Nanjing University of Aeronautics and Astronautics, Nanjing, China, in 2013 and 2016, respectively, the M.A. degree in technology management from the Technical University of Hamburg-Harburg, Hamburg, Germany, in 2016, and the Ph.D. degree from the Nanjing University of Aeronautics and Astronautics in 2020.

From 2017 to 2018, he was a Visiting Researcher with the University of Pisa, Italy. He is currently a Lecturer with the School of Electronic and Optical Engineering, Nanjing University of Science and Technology, Nanjing. He has published over 50 papers in journals and conferences. His research interests focus on frequency selective surfaces, reconfigurable metamaterials, and compatible stealth technology.

YOUYI FENG received the B.E. degree from the China University of Mining and Technology in 2021. She is currently pursuing the M.S. degree in communication engineering with the Nanjing University of Science and Technology.

Her main research interest includes liquid-based reconfigurable metamaterials.

MINXIN ZHAO received the B.S. and M.S. degrees from the Nanjing University of Aeronautics and Astronautics, Nanjing, China, in 2020 and 2023, respectively. He is currently pursuing the Ph.D. degree with the School of Electronic Science and Engineering, Nanjing University, Nanjing.

His current research interests include multifunctional active frequency selective surfaces, absorbers, and machine learning.

XIANG WANG (Member, IEEE) received the B.S. degree from the Nanjing University of Science and Technology, Nanjing, China, in 2014, and the Ph.D. degree from Southeast University, Nanjing, in 2020.

He is currently an Associate Professor with the School of Electronic and Optical Engineering, Nanjing University of Science and Technology. He has authored or coauthored over 20 papers in peer reviewed international journals. His currently research interests includes microwave and millimeter-wave passive/active components, front-end modules, and transceivers in the systems.

DANILO BRIZI (Member, IEEE) received the M.Sc. degree (summa cum laude) in biomedical engineering and the Ph.D. degree (summa cum laude) in information engineering from the University of Pisa, Italy, in 2016 and 2020, respectively.

From April 2018 to May 2019, he was a Visiting Research Scholar with the Keck School of Medicine, University of Southern California at Los Angeles, Los Angeles, USA. He is currently an Assistant Professor with the University of Pisa. His research interests include electromagnetic metasurfaces, radar absorbing materials design, and wireless power transfer applications. He was also the recipient of the Young Scientist Award during the URSI-GASS International Symposium on Electromagnetic Theory, URSI General Assembly in 2020. He was selected among the top reviewers of the IEEE TRANSACTIONS ON ANTENNAS AND PROPAGATION in 2023. Since 2022, he has been serving as an Associate Editor for the *IEEE Antennas and Propagation Magazine*.

XIAOXING FANG (Member, IEEE) received the B.S. degree from the Nanjing University of Information Science and Technology in 2013, the M.E. degree from the Jiangsu University of Science and Technology in 2016, and the Ph.D. degree from the Nanjing University of Aeronautics and Astronautics in 2021.

From 2019 to 2020, he was a Visiting Researcher with the Universitat Politècnica de Catalunya, Barcelona, Spain. He is currently a Lecturer with the Nanjing University of Information Science and Technology, Nanjing, China. His research interests include accelerated numerical methods and machine learning-based methods for solving electromagnetic problems.

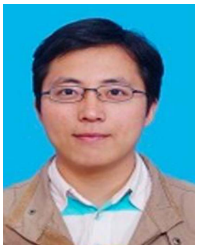

JUN HU (Member, IEEE) received the B.S., M.S., and Ph.D. degrees from Southeast University, Nanjing, China, in 2004, 2007, and 2011, respectively.

He is an Associate Professor with the School of Electronic and Optical Engineering, Nanjing University of Science and Technology, Nanjing. He has published over 30 papers in journals and conferences. His research interests include the generations and applications of vortex waves, pattern synthesizing, compact antenna array designs, computational imaging, and artificial intelligence. In 2010, he received the Best Student Paper at International Conference on Computational Problem-Solving.

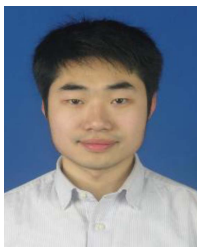

BOYU SIMA (Member, IEEE) received the B.S. and M.S. degrees from the Nanjing University of Science and Technology, Nanjing, China, in 2010 and 2013, respectively, and the Ph.D. degree from Nanjing University in 2019.

In 2019, he joined the School of Electronic and Optical Engineering, Nanjing University of Science and Technology as a Research Assistant. His research interests include metasurface, liquid crystal based antennas, and retroreflector array.

ZHIYUAN ZONG (Member, IEEE) received the B.Eng. degree in industrial automation and the Ph.D. degree in optical engineering from the Nanjing University of Science and Technology, Nanjing, China, in 1995 and 2000, respectively.

From 2012 to 2013, she was a Visiting Scholar with California State University at Northridge, Northridge, CA, USA, and the University of Houston, Houston, TX, USA. Since 2000, she has been with the School of Electronic Engineering and Photoelectric Technology, Nanjing University of Science and Technology, where she is currently a Professor. Her research interests include computational electromagnetic, modeling and design of frequency selective surfaces, antennas, and microwave systems.

WEN WU (Senior Member, IEEE) received the Ph.D. degree in electromagnetic field and microwave technology from Southeast University, Nanjing, China, in 1997.

He is currently a Professor with the School of Electronic and Optical Engineering, Nanjing University of Science and Technology, where he is also an Associate Director with the Ministerial Key Laboratory of JGMT. He has authored or coauthored over 300 journal articles and conference papers, and has submitted over 30 patent applications. His current research interests include microwave and millimeter-wave theories and technologies, microwave and millimeter-wave detection, and multimode compound detection. He was a recipient of the Six Times of Ministerial and Provincial-Level Science and Technology Awards.

AGOSTINO MONORCHIO (Fellow, IEEE) is a Full Professor with the University of Pisa. He spent several research periods with the Electromagnetic Communication Laboratory, The Pennsylvania State University, USA, both as a recipient of a scholarship (Fellowship Award) of the Summa Foundation, New Mexico, USA, and in the framework of CNR-NATO Senior Fellowship Programme. He is the Head of RaSS National Laboratory, Consorzio Nazionale Interuniversitario per le Telecomunicazioni. He has carried out a considerable research activity and technical consultancy to national, EU and U.S. industries, coordinating, as a principal scientific investigator and a large number of national and European research projects. He is active in a number of areas, including computational electromagnetics, microwave metamaterials, radio propagation for wireless systems, the design and miniaturization of antennas and electromagnetic compatibility, biomedical applications of RF and microwaves. The activity is mainly carried out with the Microwave and Radiation Laboratory, Department of Information Engineering, University of Pisa, together with a large group of Ph.D. students, Postdoctorals, and research associates. His research results have been published in more than 170 journal papers and book chapters, and more than 260 communications at international and national conferences, he is the coauthor of four patents.

Prof. Monorchio serves as reviewer for international journals, and he was an Associate Editor of IEEE ANTENNAS AND WIRELESS PROPAGATION LETTERS from 2002 to 2007. In 2012, he has been elevated to Fellow grade by the IEEE for his contributions to computational electromagnetics and for application of frequency selective surfaces in metamaterials. He is a member of the Scientific Advisory Board of Directed Energy Research Center of TII, Abu Dhabi, UAE, and affiliated with the Pisa Section of INFN, the National Institute of Nuclear Physics.